Research Square

Preprints are preliminary reports that have not undergone peer review.
They should not be considered conclusive, used to inform clinical practice,
or referenced by the media as validated information.

Influence of Poisson Effect of Compression Anchor Grout on Interfacial Shear Stress

tu bingxiong (tubingxiong@163.com)
Huq.edu.cn https://orcid.org/0000-0003-0640-5730
Liu Chao
Huaqiao University
Zhang Lihua
Dalian University of Technology
Wang Haitao
Dalian Jiaotong University

Research Article

Keywords: compression anchor, Poisson effect, interfacial shear stress, influence coefficient of Poisson effect

Posted Date: May 28th, 2021

DOI: https://doi.org/10.21203/rs.3.rs-517050/v1

License: This work is licensed under a Creative Commons Attribution 4.0 International License.
Read Full License

Version of Record: A version of this preprint was published at Geotechnical and Geological Engineering on August 15th, 2021. See the published version at https://doi.org/10.1007/s10706-021-01931-8.

Influence of Poisson Effect of Compression Anchor Grout on Interfacial Shear Stress

Bingxiong Tu[a,b], Chao Liu[a], Lihua Zhang[b], Haitao Wang[c]

[a] *Fujian engineering technology research center for tunnel and underground space, Huaqiao University, Xiamen Fujian 361021, People's Republic of China.*

[b] *State Key Laboratory of Coastal and Offshore Engineering, Dalian University of Technology, Dalian, Liaoning 116024, People's Republic of China.*

[c] *School of Civil and Safety Engineering, Dalian Jiaotong University, Dalian Liaoning 116028, People's Republic of China.*

∗ Correspondence: tubingxiong@163.com; Tel.:+86-592-6162698; Fax: +86-592-6162692

Abstract: The distribution and magnitude of the shear stress at the interface between the grout of a compression anchor rod and rock are strongly affected by the Poisson effect. To quantitatively analyze the influence of the Poisson effect on the interfacial shear stress of compression anchor rods, the equations for calculating the axial force and interfacial shear stress at the grout cross section in the anchorage section are derived in this paper, accounting for the Poisson effect of the grout. Based on the analytical solution, a new equation of the influence coefficient of the Poisson effect is proposed to quantitatively evaluate the influence of the Poisson effect on the interfacial shear stress. Distributions of the interfacial shear stress and the influence coefficient of the Poisson effect are analyzed with different parameter values. There is a neutral point in the anchorage section near the bearing plate, at which the magnitude of the shear stress is not affected by the Poisson effect. When the Poisson effect is considered, the interfacial shear stress from the neutral point to the bearing plate increases, and the distribution curve becomes steep. However, the interfacial shear stress far from the neutral point is low, and the distribution curve

becomes smooth. Overall, the Poisson effect leads to a more nonuniform distribution of the shear stress at the interface of the compression anchor rod. A larger Poisson's ratio, smaller elastic modulus, and smaller diameter of the grout lead to a greater influence of the Poisson effect. Furthermore, a larger elastic modulus of rock leads to a greater influence of the Poisson effect. The Poisson's ratio of rock and that of grout both affect the Poisson effect greatly, but the influence of the variation in the Poisson's ratio of rock on the Poisson effect is negligible. A larger interface friction angle leads to a greater influence of the Poisson effect.

Key words: compression anchor; Poisson effect; interfacial shear stress; influence coefficient of Poisson effect

---

1 Introduction

Various types of anchors are frequently used in civil engineering, such as retaining walls (Matin et al, 2019), slopes (Sawwaf and Mostafu, 2007), anti-float foundation mats (Liu et al, 2005), and tiebacks during excavation (Min-Woo et al, 2005). Marcon et al. (2017) performed tests on bonded anchors with various configurations along with a complete concrete characterization at the same concrete age. Zhao et al. (2018) determined the three-dimensional axisymmetric failure mechanism of shallow horizontal circular plate anchors that are subjected to the ultimate pullout capacity, based on the nonlinear Mohr-Coulomb failure criterion and the associated flow patterns. Sakai and Tanaka (2007) evaluated the behavior and scale effect of shallow circular anchors in two-layered sand by comparing the results of a conventional model test with the results of finite-element analysis. O'Kelly et al. (2014) described a program of field testing and numerical modeling of the pullout resistance of granular anchor installations in over-consolidated clay for an undrained condition. Merifield (2011) used numerical modeling

techniques to analyze multiplate circular anchor foundation behavior in clay soil, and studied the undrained uplift behavior of helical anchors in clays using the centrifuge model test and a "large-deformation, finite-element" approach (Wang et al, 2013). In contrast, many researchers have investigated the performance of tension anchors because of their wide use as foundations to provide uplift or lateral resistance. Su and Fragaszy (1988) conducted comparison tests of 18 ground anchors vertically buried in sand to determine the influence of factors such as diameter, fixed anchor length, and buried depth on the uplift capacity of anchors. Serrano and Olalla (1999) obtained the tensile resistance of rock anchors using the Euler's variational method and assuming a rock mass failure criterion of Hoek and Brown type. Zhang et al. (2001) investigated the tensile behavior of fiber-reinforced polymer (FRP) ground anchors. Xiao and Chen (2008) studied the load transfer mechanism of the tension-type anchor and analyzed the mechanical characteristic of an anchorage segment based on elasto-plastic theory. Ivanovic and Neilson (2009) presented a study in which the dynamic modeling of the debonding of the proximal end of the fixed anchor length of an anchorage was considered. Additionally, Liao et al. (1994) and Liu et al (2017) conducted full-scale pullout tests to focus on the behavior of ground anchors under ultimate load conditions.

In recent years, for corrosion protection of permanent anchors, compression anchors have been used due to their better corrosion protection, because whole strands are covered by sheaths filled with grease and they have less susceptibility to creep than tension anchors. In addition, in cases where anchors are installed adjacent to existing buildings or planned subway lines, there is an increasing use of compression anchors, which can be removed from the ground after construction to avoid forming underground obstacles.

Few in-depth studies have been done on the performance of compression anchors. Kim

(2003) performed anchor pull-out tests on seven instrumented full-scale low-pressure grouted anchors installed in weathered soil for three tension type anchors and four compression type anchors, which were 165 mm in diameter and embedded at a depth of 9 to 12 m. Based on the measurements, a load transfer mechanism for tension and compression ground anchors was investigated and evaluated by a simple beam spring numerical model. Liao and Hsu (2003) developed a numerical model for blade-under-reamed anchors in silty sand to evaluate the uplift behavior of anchors, and compared the calculated results to those from full scale anchor pull-out tests. Hsu and Chang (2007) performed 17 full-scale pull-out testes for vertical anchors in gravel formation, including tension, compression, and compound types of anchors. Bruce et al. (2007) described the design and construction of single-bore multiple anchors, lift-off testing procedures and results, and conclusions. Lee et al. (2012) investigated the effect of pressurized grouting on pull-out resistance and the group effect of the compression ground anchor by performing pilot-scale laboratory chamber tests and field tests. Although several previous studies of compression anchors have been conducted, the Poisson effect of compression anchor grout has not been properly taken into consideration in the aforementioned studies. However, due to the Poisson effect of the grout of the compression anchor rod, the grout near the bearing plate undergoes radial expansion under the compression of the bearing plate, causing the grout and rock mass to be squeezed at the interface, the normal stress at the interface to increase, and the interfacial shear stress to increase within this range. Therefore, the calculated bearing load of the grout near the bearing plate is larger than that when the Poisson effect is not considered, and the calculated bearing load of the grout far from the bearing plate becomes lower, thereby causing the shear stress at the interface between the grout and the rock mass far from the bearing plate to decrease.

In this paper, the formulas of the axial force on the cross-section of the anchorage body and the interfacial shear stress considering the Poisson effect are first derived. Next, a new equation of the influence coefficient of the Poisson effect is proposed to quantitatively evaluate the influence of the Poisson effect on the interfacial shear stress. Finally, in-depth analysis is conducted of the distribution of the interfacial shear stress and the influence coefficient of the Poisson effect with different parameter values.

2 Theoretical derivation

2.1 General Assumptions

To facilitate the theoretical analysis and derivations, the following assumptions for compression anchors are made. (1) The shear stress and shear displacement on the surface of the grout have a linear elastic relation, and the shear displacement on the surface of the grout is equal to the displacement on the cross-section of the grout at the corresponding location. (2) The anchor can be freely and elastically elongated in the sheath, and there is no friction between the anchor rod and the sheath. (3) The axial stress is uniformly distributed on the cross-section of the grout. (4) The rock is isotropic and homogeneous. (5) The thickness of the bearing plate is not considered.

2.2 Theoretical Solution

Taking the location of the bearing plate of the compression anchor as the origin of the coordinates, a one-dimensional rectangular coordinate system is established along the direction of the anchor head, as shown in Figure 1.

Since the grout is not an ideal rigid body, the grout will undergo radial expansion within a certain range due to the Poisson effect when its bottom end is squeezed by the bearing plate. Hence, a radial stress σ_r will be generated at the interface between the grout and the rock,

improving the interfacial bond strength to some extent. A micro-element from the grout of the anchorage body is shown in Figure 1, and a corresponding stress analysis diagram is established, as shown in Figure 2.

Based on static equilibrium, the following equation is satisfied:

$$\tau_1(x) = -\frac{1}{\pi D} \cdot \frac{\mathrm{d}P_1(x)}{\mathrm{d}x} \tag{1}$$

where $\tau_1(x)$ is the shear stress at the interface between the grout and the rock (kPa), $P_1(x)$ is the axial force on the cross-section of the grout (kN), and D is the diameter of the grout (m).

For a tension anchor, the relation between the shear stress at the grout–rock interface and the composite shear stiffness of the interface can be established using the shear force intensity as follows:

$$q(x) = \pi D \tau(x) = K_s w(x) \tag{2}$$

where $q(x)$ is the shear force per unit length of the anchorage body of the tension anchor (kN/m), $w(x)$ is the interfacial shear displacement of the anchorage body of the tension anchor rod (m), and K_s is the composite tangent stiffness of the interface between the grout body and the rock (kPa). The physical meaning of K_s is the shear force per unit length required at the interface to produce a unit shear displacement on the corresponding interface, which can be calculated using the shear stiffnesses of the grout and the rock proposed by Oda et al. (1997):

$$\frac{1}{K_s} = \frac{1}{K_b} + \frac{1}{K_r} \tag{3}$$

where K_b is the shear stiffness of the grout, and K_r is the shear stiffness of the rock.

As Chou and Pagano (1992) proposed, the shear stiffness K_b of the grout can be obtained by considering the equation for a thick-walled cylinder from the theory of elasticity:

$$K_b = \frac{2\pi G_g}{\ln(D/d)} \tag{4}$$

where G_g is the shear modulus of the grout, which is defined herein as $G_g = \frac{E_g}{2(1+\mu_g)}$, E_g is the elastic modulus of the grout, μ_g is the Poisson's ratio of the grout, and d is the diameter of the strand.

For the compression anchor, due to the Poisson effect, the shear force intensity of the grout can be decomposed into two parts: that caused by the interfacial shear displacement and that caused by the interfacial radial stress. The shear force intensity can be expressed as follows:

$$q_1(x) = \pi D \tau_1(x) = K_s w_1(x) + \pi D \sigma_r(x) \tan\delta \tag{5}$$

where $q_1(x)$ is the shear force per unit length of the grout of the compression anchor (kN/m), $w_1(x)$ is the interfacial shear displacement of the grout at the coordinate x of the anchorage body of the compression anchor (m), $\sigma_r(x)$ is the radial stress at the interface between the grout and the rock (kPa), and δ is the interface friction angle (°) between the grout and the rock.

For the compression anchor, the shear displacement $w_1(x)$ of the grout interface at the coordinate x of the anchorage body in Figure 1 can be expressed by Hooke's law (Chou and Pagono, 1992) as follows:

$$w_1(x) = \frac{1}{E_g A_g} \int_x^{l_a} P_1(x) dx \tag{6}$$

where A_g is the net bearing area of the grout, $A_g = \frac{1}{4}\pi(D^2 - d^2)$, and l_a is the total length of the anchorage body.

Taking the derivative of Equation (6) with respect to x yields the following:

$$P_1(x) = -E_g A_g \frac{dw_1(x)}{dx} \tag{7}$$

Solving Equations (1), (5), and (7) simultaneously yields the following:

$$\frac{d^2 w_1(x)}{dx^2} - \frac{4D\sigma_r(x)\tan\delta}{(D^2 - d^2)E_g} - \frac{4K_s w_1(x)}{\pi(D^2 - d^2)E_g} = 0 \tag{8}$$

According to the physical equation in cylindrical coordinates of the space problem from elasticity theory (Chou and Pagono, 1992), we have the following:

$$\varepsilon_\rho = \frac{1}{E} \cdot [\sigma_\rho - \mu(\sigma_\varphi + \sigma_x)] \tag{9}$$

According to the third assumption, $\sigma_\varphi = \sigma_\rho = \sigma_r$, which is substituted into Equation (9), resulting in the following:

$$\varepsilon_\rho = \frac{\mu_g \sigma_x - (1-\mu_g)\sigma_r}{E_g} \tag{10}$$

where ε_ρ is the radial strain of the grout, and σ_x is the normal stress on the cross-section of the grout.

According to the theory of elasticity, when a circular hole with a radius R on an infinite plane is subjected to a uniform internal pressure σ_r, the radial displacement of the hole wall is as follows:

$$u_\rho = \frac{(1+\mu)R^2\sigma_r}{E \cdot \rho} \tag{11}$$

At the interface between the grout and the rock, i.e., at $\rho = R$, Equations (10) and (11) yield the following:

$$\int_0^R \frac{\mu_g \sigma_x - (1-\mu_g)\sigma_r}{E_g} \mathrm{d}\rho = \frac{(1+\mu_r)R\sigma_r}{E_r} \tag{12}$$

where μ_r is the Poisson's ratio of the rock, and E_r is the elastic modulus of the rock.

Equation (12) is integrated and rearranged, yielding the following:

$$\sigma_r = k \cdot \sigma_x \tag{13}$$

where $k = \frac{E_r \mu_g}{E_r(1-\mu_g) + E_g(1+\mu_r)}$, and $\sigma_x = \frac{P_1(x)}{A_g}$.

Substituting Equation (7) into Equation (13) yields

$$\sigma_{\mathrm{r}}(x) = -kE_{\mathrm{g}} \cdot \frac{\mathrm{d}w_1(x)}{\mathrm{d}x} \tag{14}$$

Substituting Equation (14) into Equation (8) yields the following:

$$\frac{\mathrm{d}^2 w_1(x)}{\mathrm{d}x^2} + \frac{4Dk \cdot \tan\delta}{\left(D^2 - d^2\right)} \frac{\mathrm{d}w_1(x)}{\mathrm{d}x} - \frac{4K_{\mathrm{s}}}{\pi\left(D^2 - d^2\right)E_g} w_1(x) = 0 \tag{15}$$

The characteristic equation for Equation (15) is as follows:

$$r^2 + \frac{\pi Dk \cdot \tan\delta}{A_g} r - \frac{K_{\mathrm{s}}}{E_{\mathrm{g}} A_{\mathrm{g}}} = 0 \tag{16}$$

The discriminant of Equation (16) is

$$\Delta = \left(\frac{\pi Dk \cdot \tan\delta}{A_g} \right)^2 + \frac{4K_{\mathrm{s}}}{E_{\mathrm{g}} A_{\mathrm{g}}} \tag{17}$$

If the discriminant given by Equation (17) is greater than zero, Equation (16) has two unequal real roots, r_1 and r_2, expressed as follows:

$$r_1 = -\frac{1}{2}\left(\frac{\pi Dk \cdot \tan\delta}{A_{\mathrm{g}}} - \sqrt{\Delta}\right) \tag{18}$$

$$r_2 = -\frac{1}{2}\left(\frac{\pi Dk \cdot \tan\delta}{A_{\mathrm{g}}} + \sqrt{\Delta}\right) \tag{19}$$

Thus, the general solution of Equation (15) is

$$w_1(x) = C_1 \cdot \mathrm{e}^{r_1 x} + C_2 \cdot \mathrm{e}^{r_2 x} \tag{20}$$

Substituting Equation (20) into Equation (7) and substituting the boundary conditions $P_1(x)\big|_{x=0} = P$ and $P_1(x)\big|_{x=l_{\mathrm{a}}} = 0$ yields in the following:

$$C_1 = \frac{4P}{\pi\left(D^2 - d^2\right)E_g} \cdot \frac{\mathrm{e}^{(r_2 - r_1)l_{\mathrm{a}}}}{r_1[1 - \mathrm{e}^{(r_2 - r_1)l_{\mathrm{a}}}]} \tag{21}$$

$$C_2 = -\frac{4P}{\pi\left(D^2 - d^2\right)E_g} \cdot \frac{1}{r_2[1 - \mathrm{e}^{(r_2 - r_1)l_{\mathrm{a}}}]} \tag{22}$$

Substituting Equations (20), (21), and (22) into Equation (7), we obtain the axial force

acting on the grout considering the Poisson effect:

$$P_1(x) = P \cdot \left[\frac{e^{(r_2 - r_1)l_a + r_1 x} - e^{r_2 x}}{e^{(r_2 - r_1)l_a} - 1} \right] \tag{23}$$

Solving Equations (1) and (23) simultaneously yields the shear stress at the interface between the grout and the rock considering the Poisson effect:

$$\tau_1(x) = \frac{P}{\pi D} \cdot \left[\frac{r_1 \cdot e^{(r_2 - r_1)l_a + r_1 x} - r_2 \cdot e^{r_2 x}}{1 - e^{(r_2 - r_1)l_a}} \right] \tag{24}$$

2.3 Evaluation of influence of Poisson effect

Assuming that the grout of the compression anchor only undergoes axial compression without radial deformation, the Poisson effect will not occur when the grout is compressed. In this case, it can be assumed that the Poisson's ratio of the grout is $\mu_g = 0$. Consequently, $k = 0$, and the radial stress $\sigma_r = 0$ is obtained from Equation (13). Thus, the Poisson effect of the grout of the compression anchor can be neglected.

According to Equation (17), when $k = 0$, $\Delta = \frac{4K_s}{E_g A_g}$. Equations (18) and (19) can be simplified to $r_1 = \beta$ and $r_2 = -\beta$, respectively, where $\beta = \sqrt{\frac{K_s}{E_g A_g}}$. Substituting the simplified r_1 and r_2 into Equation (23) yields the axial force on the cross-section of the anchorage body of the compression anchor when the Poisson effect of the grout is neglected:

$$P_2(x) = P \cdot \left[\frac{e^{\beta x} - e^{2\beta l_a - \beta x}}{1 - e^{2\beta l_a}} \right] \tag{25}$$

Similarly, substituting the simplified r_1 and r_2 corresponding to $\mu_g = 0$ into Equation (24) gives the interfacial shear stress of the anchorage body of the compression anchor when the Poisson effect of the grout is neglected:

$$\tau_2(x)=\frac{\beta P}{\pi D}\cdot\left[\frac{\mathrm{e}^{\beta x}+\mathrm{e}^{2\beta l_\mathrm{a}-\beta x}}{\mathrm{e}^{2\beta l_\mathrm{a}}-1}\right] \tag{26}$$

To quantitatively analyze and evaluate the influence of the Poisson effect of the grout of the compression anchor, the influence coefficient λ of the Poisson effect is defined as the ratio of the interfacial shear stress when the Poisson effect of the grout is considered to that when the Poisson effect is neglected, i.e., $\lambda=\tau_1(x)/\tau_2(x)$, which is used to analyze and evaluate the influence of the Poisson effect of the grout at different locations of the anchorage body of the compression anchor.

3 Comparative analysis of Poisson effect of grout

To comparatively analyze the influence of the Poisson effect of the grout on the distribution of the interfacial shear stress and the cross-sectional axial force, values of the tension P of the anchor head; the elastic modulus E_g, Poisson's ratio μ_g, and diameter D of the grout; the elastic modulus E_r and Poisson's ratio μ_r of the rock; the interfacial friction angle δ; the length l_a of the anchorage body; and the diameter d of the strand were specified for calculation and analysis, as summarized in Table 1.

Table 1. Values of calculated parameters

P(kN)	E_g(GPa)	μ_g	D(m)	E_r(GPa)	μ_r	δ(°)	l_a(m)	d(m)
300	10	0.25	0.15	5	0.2	25	2	0.03

Using the parameters in Table 1, Equations (24) and (26) were used to calculate the interfacial shear stress of the compression anchor with and without the Poisson effect, respectively, as shown in Figure 3. The distribution curve of the corresponding influence coefficient of the Poisson effect along the grout is also shown in Figure 3.

Figure 3 shows that the overall shapes of the shear stress distribution curves under the two

conditions are similar in that the shear stresses have maxima at the bearing plate and decrease rapidly as the distance from the bearing plate increases. The interfacial shear stress considering the Poisson effect increases first and then decreases as the distance from the bearing plate increases. The interfacial shear stress within the range of approximately 0.5 m (3.3 *D*) from the bearing plate increases significantly, with the largest increase (approximately 34.8%) at the bearing plate. After the distance from the bearing plate is more than approximately 0.5 m, the Poisson effect causes the interfacial shear stress to decrease. When the Poisson effect is neglected, the interfacial shear stress 2.0 m from the bearing plate is 0.073 MPa. When the Poisson effect is considered, the value decreases to 0.024 MPa, corresponding to a decrease of 67.1%. The location at which the interfacial shear stress decreases to 0.073 MPa is approximately 1.33 m from the bearing plate, corresponding to a length decrease of about 33.5%. Therefore, considering the Poisson effect of the grout of the compression anchor causes the interfacial shear stress to first increase and then decrease. Furthermore, compared to the case without the Poisson effect, the distribution becomes more uneven, and the length of the anchorage body mainly bearing the load decreases significantly.

λ = 1.0 indicates that the Poisson effect does not cause an increase or decrease in the interfacial shear stress at this point. The point λ = 1.0 is defined as the neutral point, and the distance from the bearing plate to the neutral point is the depth of the neutral point. Figure 3 shows that the influence coefficient λ of the Poisson effect decreases as the distance from the bearing plate increases. The depth of the neutral point is approximately 0.5 m, and $\lambda > 1.0$ within this range. This occurs because, under the influence of the Poisson effect, the grout within the depth of the neutral point is squeezed by the bearing plate, generating a strong lateral radial expansion and thereby forming a radial stress at the interface of the grout and the rock. As a

result, the interfacial bond strength is improved, and the interfacial shear stress that can be withstood increases accordingly. Thus, $\lambda > 1.0$ within the range of the neutral point depth. After the distance from the bearing plate exceeds the depth (0.5 m) of the neutral point, $\lambda < 1.0$. This occurs because the lateral expansion of the grout caused by its Poisson effect has a finite depth, and the interfacial shear stress within the range of the neutral point depth increases, leading to a decrease in the axial compression on the cross-section of the grout. Thus, the load experienced by the anchorage body beyond the depth of the neutral point decreases, causing a decrease in the interfacial shear stress, and thus, $\lambda < 1.0$.

4 Parameter influence analysis

To examine the influence of the Poisson effect of the grout on the interfacial shear stress and the influence coefficient of the Poisson effect under different parameters, different parameters were selected for comparative analysis. When the influence of a certain parameter is analyzed, the rest of parameters remain unchanged, and their values are summarized in Table 1.

4.1 Influence of Poisson's Ratio of Grout

The Poisson's ratio μ_g of the grout was set to 0.25, 0.30, and 0.35. The corresponding distributions of the interfacial shear stress and influence coefficient of the Poisson effect are shown in Figures 4a and 4b, respectively.

Figure 4a shows that when the Poisson effect is considered, the interfacial shear stress increases first and then decreases with the increasing distance from the bearing plate, and the overall distribution is more uneven than that of the case without the Poisson effect. Within the range of the neutral point depth of 0.5 m (3.3 D), the interfacial shear stress increases with increasing μ_g. This indicates that a larger μ_g corresponds to a greater lateral expansion of the grout at the same level of axial deformation, a higher interfacial radial stress, a greater interfacial

bond strength, and a larger interfacial shear stress resisted between the grout and rock. Beyond the neutral point, the interfacial shear stress decreases with increasing μ_g. Therefore, the larger μ_g is, the greater the influence of the Poisson effect is, and the more uneven the distribution of the interfacial shear stress becomes.

When the Poisson effect is neglected, the interfacial shear stress at the bearing plate is 1.079 MPa. After the Poisson effect of the grout is considered, when μ_g is 0.25, 0.30, and 0.35, the interfacial shear stresses at the bearing plate increase to 1.455, 1.549, and 1.650 MPa, respectively, corresponding to increases of 34.8%, 43.6%, and 52.9%. When the Poisson effect is neglected, the interfacial shear stress 2.0 m from the bearing plate is 0.073 MPa. After the Poisson effect is considered, when μ_g is 0.25, 0.30, and 0.35, the distances from the bearing plate corresponding to the decrease in the interfacial shear stress to 0.073 MPa are 1.33, 1.27, and 1.21 m, respectively, corresponding to length decreases of approximately 33.5%, 36.5%, and 39.5%. This indicates that the Poisson effect of the grout reduces the length of the anchorage body that mainly bears the load, and a larger value of μ_g corresponds to a smaller length of the anchorage body that mainly bears the load.

Figure 4b shows that the influence coefficient of the Poisson effect λ decreases as the distance from the bearing plate increases, and the larger the value of μ_g is, the greater the influence of the Poisson effect becomes. The depths of the neutral point are consistent for different μ_g values and are approximately 0.5 m (3.3D). Within the range of the neutral point depth, the larger the value of μ_g is, the higher the value of λ becomes, which is always greater than 1.0. When μ_g is equal to 0.25, 0.30, and 0.35, the λ values at the bearing plates are 1.348, 1.435, and 1.529, respectively. Beyond the neutral point, a larger value of μ_g corresponds to a smaller λ, which is always less than 1.0.

4.2 Influence of Elastic Modulus of Grout

The elastic modulus of the grout E_g was set to 5, 10, and 15 GPa, and the distribution curves of the corresponding shear stress and influence coefficient of the Poisson effect are shown in Figures 5a and 5b.

Figure 5a shows that when the Poisson effect is considered, the interfacial shear stress increases first and then decreases with increasing distance from the bearing plate. Furthermore, compared to the case without the Poisson effect, the overall distribution is more uneven, and a smaller E_g results in a more uneven distribution curve of the interfacial shear stress. Within the range of the neutral point depth, the interfacial shear stress increases with decreasing E_g. This is because a smaller elastic modulus of the grout corresponds to a larger axial deformation under compression, a larger lateral expansion, and a higher interfacial radial stress. This leads to a greater interfacial bond strength and a higher shear stress that can be withstood. Beyond the neutral point, the interfacial shear stress decreases with deceasing E_g.

When the Poisson effect is neglected and E_g is 5, 10, and 15 GPa, the interfacial shear stresses at the bearing plate are 1.500, 1.079, and 0.891 MPa, respectively. When the Poisson effect is considered, the corresponding interfacial shear stresses at the bearing plate increase to 2.119, 1.455, and 1.158 MPa, respectively, corresponding to increases of 41.3%, 34.8%, and 30.0%, respectively. When the Poisson effect is neglected and E_g is 5, 10, and 15 GPa, the interfacial shear stresses at 2.0 m from the bearing plate are 0.027, 0.073, and 0.111 MPa, respectively. When the Poisson effect is considered, the distances from the bearing plate to the locations where the interfacial shear stress decreases to these values are approximately 1.31, 1.33, 1.34 m, respectively, corresponding to reductions in length of approximately 34.5%, 33.5%, and 33.0%. This indicates that the Poisson effect of the grout greatly reduces the length of the

anchorage body that mainly bears the load, but the variation of E_g has little influence on the extent of the decrease in the length.

Figure 5b shows that when the Poisson effect is considered, within a certain range from the bearing plate, the influence coefficient of the Poisson effect λ decreases with increasing elastic modulus of the grout E_g. However, beyond this range from the bearing plate, λ increases as E_g increases. When E_g is 5, 10, and 15 GPa, the depths of the neutral point are approximately 0.36 (2.4 D), 0.50 (3.3 D), and 0.60 m (4.0 D), respectively, and the values of λ at the bearing plate are 1.413, 1.348, and 1.300, respectively. This indicated that the larger E_g is, the greater the depth of the lateral expansion of the grout is, and the smaller λ is at the bearing plate.

4.3 Influence of Grout Diameter

The diameter D of the grout was set to 0.10, 0.15, and 0.20 m, respectively, and the distribution curves of the corresponding shear stress and influence coefficient of the Poisson effect are shown in Figures 6a and 7b.

Figure 6a shows that when the Poisson effect is considered, the interfacial shear stress increases first and then decreases as the distance from the bearing plate increases, and the overall distribution is more uneven than that of the case without the Poisson effect. A larger diameter of the grout corresponds to a more gradually varying distribution curve of the interfacial shear stress and a lower peak shear stress at the interface of the bearing plate. This occurs because a larger diameter corresponds to a larger area of the interface between the grout and the rock and a smaller load per unit interface area. Thus, the interfacial shear stress concentration near the bearing plate is greatly reduced. As a result, the peak shear stress is significantly reduced, the distribution curve of the shear stress along the length of the anchorage body is more uniform, and the curve varies more gradually.

When the Poisson effect is neglected and D is taken as 0.10, 0.15, and 0.20 m, the interfacial shear stresses at the bearing plate are 2.498, 1.079, and 0.607 MPa, respectively. When the Poisson effect is considered, the interfacial shear stresses at the bearing plate increase to 3.393, 1.455, and 0.813 MPa, respectively, corresponding to increases of 35.8%, 34.8%, and 33.9%. When the Poisson effect is neglected and D is set to 0.10, 0.15, and 0.20 m, the interfacial shear stresses 2.0 m from the bearing plate are 0.027, 0.073, and 0.098 MPa, respectively. In comparison, when the influence of the Poisson effect is considered, the distances from the bearing plate to the locations where the interfacial shear stresses are reduced to these values decrease to approximately 1.36, 1.33, and 1.30 m, respectively, corresponding to length reductions of approximately 32.0%, 33.5%, and 35.0%. This indicates that the Poisson effect of the grout greatly decreases the length of the anchorage body that mainly bears the load, but the extent of the decrease increases only slightly with increasing diameter.

Figure 6b shows that overall the influence coefficient of the Poisson effect λ increases as the diameter of the grout increases, but the extent of the increase is significantly reduced. When D is 0.10, 0.15, and 0.20 m, the depths of the neutral point are approximately 0.33 m (3.3 D), 0.50 m (3.3 D), and 0.65 m (3.3 D), respectively. This indicates that a larger diameter corresponds to a larger depth of the lateral expansion of the grout caused by the Poisson effect. However, the ratio of the lateral expansion depth to the grout diameter remains unchanged.

4.4 Influence of Poisson's Ratio of Rock

The Poisson's ratio of the rock was set to 0.1, 0.2, and 0.3. The distribution curves of the corresponding shear stress and influence coefficient of the Poisson effect are shown in Figures 7a and 7b.

Figure 7a shows that when the Poisson effect is considered, the interfacial shear stress

increases first and then decreases as the distance from the bearing plate increases, and the overall distribution is more uneven than that when the Poisson effect is neglected. When the Poisson effect is considered, within the range of the neutral point depth, the interfacial shear stress decreases slightly with increasing Poisson's ratio μ_r. Meanwhile, at the bearing plate with μ_r equal to 0.1 and 0.3, the interfacial shear stresses are 1.483 and 1.430 MPa, respectively, corresponding to a relative difference of only 3.6%. Therefore, the variation of μ_r has little (almost negligible) effect on the interfacial shear stress.

Figure 7b shows that the influence coefficient of the Poisson effect varies little with the Poisson's ratio of the rock. When μ_r is equal to 0.1, 0.2, and 0.3, respectively, λ at the bearing plate is 1.375, 1.348, and 1.325, respectively, amounting to a maximum relative difference of only 3.6%. Thus, the influence of the variation of the Poisson's ratio is basically negligible. The values of λ 2.0 m from the bearing plate are 0.295, 0.321, and 0.345, respectively, amounting to a maximum relative difference of 14.5%. However, considering that the interfacial shear stress at the end is very small (close to zero), the influence of the variation of the Poisson's ratio of the rock on the Poisson effect of the grout can also be neglected.

4.5 Influence of Elastic Modulus of Rock

The elastic modulus of the rock E_r was set to 1, 5, and 10 GPa. The distributions of the corresponding shear stress and coefficient distribution of the Poisson effect are shown in Figures 8a and 8b.

Figure 8a shows that, when the Poisson effect is considered, the interfacial shear stress increases first and then decreases with increasing distance from the bearing plate, and the distribution curve is more uneven than that with the Poisson effect neglected. At the bearing plate, the increase of the interfacial shear stress caused by the Poisson effect improves with increasing

E_r. This occurs because, under the same lateral expansion, a greater elastic modulus of the rock corresponds to a stronger ability to restrain the lateral expansion deformation of the grout, leading to a higher interfacial radial stress and hence a higher shear stress. In comparison, beyond a certain distance from the bearing plate, the interfacial shear stress decreases with increasing E_r.

When the Poisson effect is neglected and E_r is 1, 5, and 10 GPa, the interfacial shear stresses at the bearing plate are 0.706, 1.079, and 1.500 MPa, respectively. When the Poisson effect is considered, the interfacial shear stresses at the bearing plate increase to 0.791, 1.455, and 2.19 MPa, respectively, corresponding to increases of 12.0%, 34.8%, and 41.3%. When the Poisson effect is neglected and E_r is 1, 5, and 10 GPa, the interfacial shear stresses 2.0 m from the bearing plate are 0.161, 0.073, and 0.027 MPa, respectively. In comparison, when the influence of the Poisson effect is considered, the distances from the bearing plate to the locations where the interfacial shear stress decreases to these values are approximately 1.49, 1.33, and 1.31 m, respectively, corresponding to decreases in length of approximately 25.5%, 33.5%, and 34.5%. This indicates that the Poisson effect of the grout greatly reduces the length of the anchorage body that mainly bears the load, and the extent of the decrease increases with the increasing elastic modulus of the rock.

Figure 8b shows that the influence coefficient of the Poisson effect λ is greatly affected by the elastic modulus of the rock. Overall, a smaller value of E_r corresponds to a more gradually varying λ curve, indicating less variation of the interfacial shear stress caused by the Poisson effect of the grout along the anchorage body length. At the bearing plate, λ is 1.121 (E_r = 1 GPa), 1.348 (E_r = 5 GPa), and 1.413 (E_r = 10 GPa), i.e., λ increases as E_r increases. When E_r is 1, 5, and 10 GPa, the distances from the neutral point to the bearing plate are approximately 0.75 m (5 D),

0.50 m (3.3 D), and 0.30 m (2 D), respectively. This indicates that a smaller value of E_r corresponds to a larger depth of the lateral expansion of the grout caused by the Poisson effect and a larger range of increase in the interfacial shear stress.

4.6 Influence of Interface Friction Angle

The interface friction angle δ was set to 15°, 25°, and 35°, and the distributions of the corresponding shear stress and influence coefficient of the Poisson effect are shown in Figures 9a and 9b.

Figure 9a shows that when the Poisson effect is considered, the interfacial shear stress increases first and then decreases as the distance from the bearing plate increases, and the overall distribution is more uneven than that when the Poisson effect is neglected. Within the range of the neutral point depth, the larger the interface friction angle is, the higher the interfacial shear stress becomes, i.e., the greater the extent of the increase in the interfacial shear stress caused by the Poisson effect is. Beyond the depth of the neutral point, the larger the interface friction angle is, the lower the interfacial shear stress is, and the larger the extent of the decrease in the interfacial shear stress caused by the Poisson effect becomes.

When the Poisson effect is neglected, the interfacial shear stress at the bearing plate is 1.079 MPa. When the Poisson effect is considered and δ is equal to 15°, 25°, and 35°, the corresponding interfacial shear stresses at the bearing plate increase to 1.283, 1.455, and 1.677 MPa, respectively, corresponding to increases of 18.9%, 34.8%, and 55.4%. When the Poisson effect is neglected, the interfacial shear stress 2.0 m from the bearing plate is 0.073 MPa. However, when the Poisson effect is considered and δ is equal to 15°, 25°, and 35°, the distances from the bearing plate to the corresponding locations where the interfacial shear stress decreases to 0.073 MPa are approximately 1.47, 1.33, and 1.20 m, respectively, corresponding to

reductions in length of approximately 26.5%, 33.5%, and 40.0%. This indicates that the Poisson effect of the grout reduces the length of the anchorage body that mainly bears the load, and the extent of reduction improves as the interface friction angle increases.

Figure 9b shows that within the range of the neutral point depth, the influence coefficient of Poisson effect λ increases with increasing δ. Beyond this range, λ decreases with increasing δ. When δ is equal to 15°, 25°, and 35°, the depths of the neutral point are approximately 0.55 m (3.7 D), 0.50 m (3.3 D), and 0.45 m (3 D), respectively. This indicates that a larger δ corresponds to a smaller depth of the lateral expansion of the grout caused by the Poisson effect but a larger extent of increase in the interfacial shear stress.

5 Conclusions

The purpose of this study is to evaluate the influence of the Poisson effect of compression anchor grout. Formulas are derived for the axial force on the cross-section of the anchorage body and the interfacial shear stress between the grout and rock considering the Poisson effect. Then, an influence coefficient of the Poisson effect is proposed to estimate the influence of the Poisson effect. Distributions of the interfacial shear stress and the influence coefficient of the Poisson effect are analyzed with different parameter values. The results under the conditions of this study can be summarized as follows.

(1) The Poisson effect of compression anchor grout results in increased interfacial shear stress between the grout and rock within the depth of the neutral point, and in reduced interfacial shear stress far from the neutral point. Distribution of the interfacial shear stress becomes more uneven, and the length of the anchorage body mainly bearing the load decreases significantly, in contrast to the case without the Poisson effect.

(2) A larger Poisson's ratio, smaller elastic modulus, and smaller diameter of the grout lead

to a greater influence of the Poisson effect. Furthermore, a larger elastic modulus of the rock leads to a greater influence of the Poisson effect. The Poisson's ratio of rock and that of grout both affect the Poisson effect greatly, but the influence of the variation in the Poisson's ratio of the rock on the Poisson effect is negligible. A larger interface friction angle leads to a greater influence of the Poisson effect.

Acknowledgements

This work was supported by the Open Fund of State Key Laboratory of Coastal and Offshore Engineering, Dalian University of Technology with grant No. LP2013, the National Key R&D Program of China with Grant No. 2018YFC1505300-2, and the National Natural Science Foundation of China with Grant Nos. 51408424 and 51678112.

References

Bruce, M.; Gómez, J.; Traylor, R. Repeated lift-off testing of single bore multiple anchors for Dam retaining wall over a 5-year period. Institution of Civil Engineers - International Conference on Ground Anchorages and Anchored Structures in Service 2007, 2007, 111-119.

Chou, P.; Pagano, N. Elasticity: Tensor, Dyadic and Engineering Approaches. New York. Dover Publications Inc. 1992.

Hsu, S.; Chang, C. Pullout performance of vertical anchors in gravel formation. *Eng. Geol.* 2007, 90, 17-29.

Ivanovic, A.; Neilson, R. Modelling of debonding along the fixed anchor length. *Int. J. Rock Mech. Min.* 2009, 46, 699-707.

Kim, N. Performance of tension and compression anchors in weathered soil. *J. Geotech. Geoenviron*. 2003, 129: 1138–1150.

Lee, S.; Kim, T.; Sim, B.; Kin, J.; Lee, I. Effect of pressurized grouting on pullout resistance and group efficiency of compression ground anchor. *Can. Geotech. J.* 2012, 49, 939-953.

Liao, H.; Hsu, S. Uplift behavior of blade-underreamed anchors in silty sand. *J. Geotech. Geoenviron.* 2003, 129, 560-568.

Liao, H.; Ou, C.; Shu, S. Anchorage behavior of shaft anchors in alluvial soil. *J. Geotech. Geoenviron.* 1994, 122, 526-533.

Liu, J.; Wu, P.; Yin, H.; Zhong, D.; Li, S.; Zhou, H.; Li, Z.; Xu, H. Pressure-dispersive anti-float anchor technique and its application to engineering, *Chinese Journal of Rock Mechanics and Engineering*, 2005, 24, (in Chinese).

Liu, X.; Wang, J.; Huang, J.; Jiang, H. Full-scale pullout tests and analyses of ground anchors in rocks under ultimate load conditions. *Eng. Geol.* 2017, 228, 1-10.

Marcon, M.; Vorel, J.; Ninˇcevi´c, K.; Wan-Wendner, W. Modeling adhesive anchors in a discrete element framework. *MATERIALS*. 2017, 10, 917-929.

Merifield, R. Ultimate uplift capacity of multiplate helical type anchors in clay. *J. Geotech. Geoenviron.* 2011, 137, 704-716.

Matin, M.; Amirali, Z.; Nima, M.; Nader, D. Experimental study on the performance of plate anchor retaining walls. *Int. J. Phys. Model. Geo.* 2019, 19, 128-140.

Min-Woo, S.; Scott, M.; Ku Seung, Y.; Myoung-Mo, K. Sequential analysis of ground movements at three deep excavation sites with mixed ground profiles. *J. Geotech .Geoenviron*. 2010, 136, 656-668.

Oda, H.; Zhang, M.; Skimayanma, M. Study on load-dispersive anchorage and shear stress in surrounding soils. Proceedings of international conference on application and development of rock-soil anchoring technology. Liuzhou, 1997, 237-244.

O'Kelly, B.; Brinkgreve, R.; Sivakumar, V. Pullout resistance of granular anchors in clay for undrained condition. *Soils Found.* 2014, 54, 1145-1158.

Sakai, T.; Tanaka, T. Experimental and Numerical Study of Uplift Behavior of Shallow Circular Anchor in Two-Layered Sand. *J. Geotech. Geoenviron.* 2007, 133, 469-477.

Sawwaf, E.; Mostafa, A. Uplift behavior of horizontal anchor plates buried in geosynthetic reinforced slopes. *Geotech. Test J.* 2007, 30, 418-426.

Serrano, A.; Olalla, C. Tensile resistance of rock anchors. *Int. J. Rock Mech. Min*. 1999, 36, 449-474.

Su, W.; Fragaszy, R. Uplift testing of model anchors. *J. Geotech. Geoenviron.* 1988, 114, 961-983.

Wang, D.; Merifield, R.; Gaudin, C. Uplift behaviour of helical anchors in clay. *Can. Geotech. J.* 2013, 50, 575-584.

Xiao, S.; Chen, C. Mechanical mechanism analysis of tension type anchor based on shear displacement method. *J. Cent. South Univ. T*. 2008, 15, 106-111.

Zhang, B.; Benmokrane, B.; Chennouf, A.; Mukhopadhyaya, P.; El-Safty, A. Tensile behavior of FRP tendons for prestressed ground anchors. *J. Compos. Constr.* 2001, 5, 85-93.

Zhao, L.; Tan, Y.; Hu, S.; Deng, D.; Yang, X. Upper bound analysis of ultimate pullout capacity of shallow 3-D circular plate anchors based on nonlinear Mohr-Coulomb failure criterion. *J. Cent. South Univ.T.* 2018, 25, 2272-2288.

Figures

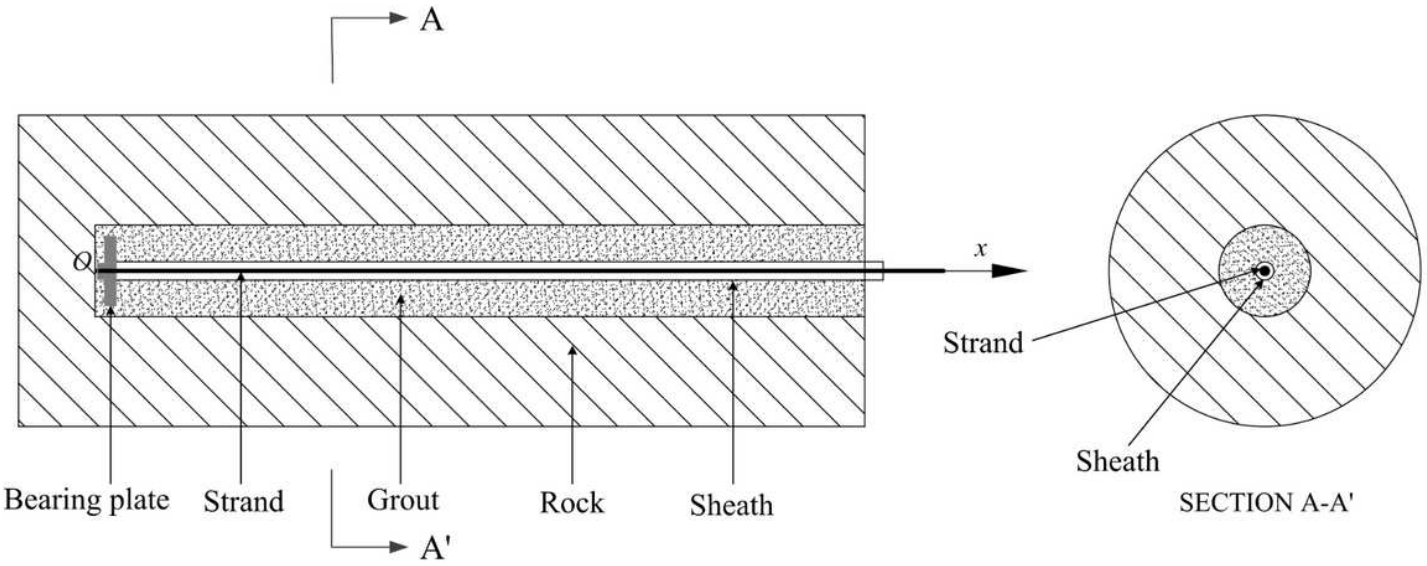

Figure 1

Compression anchor.

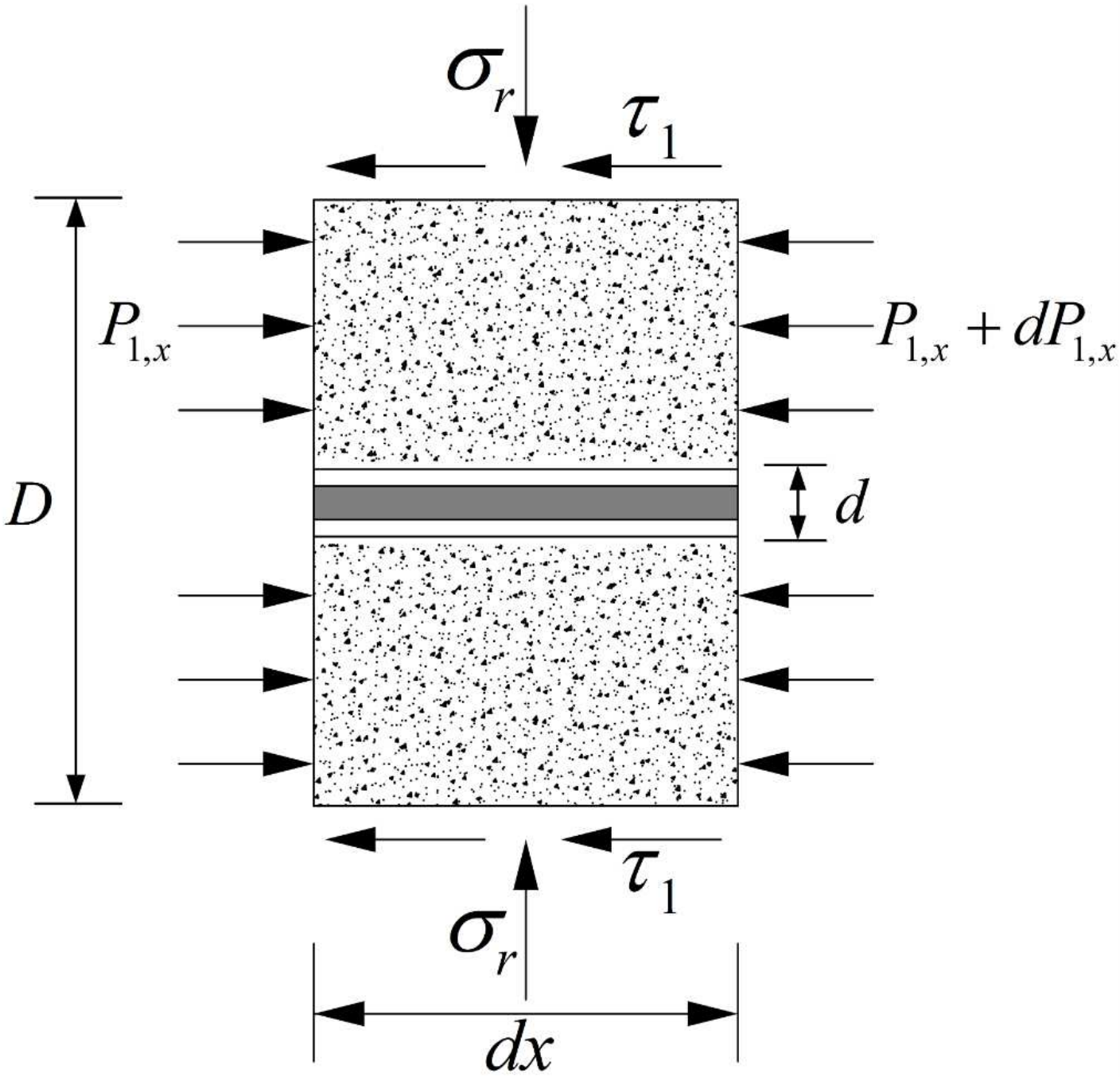

Figure 2

Stress analysis diagram of micro elements for the anchorage body.

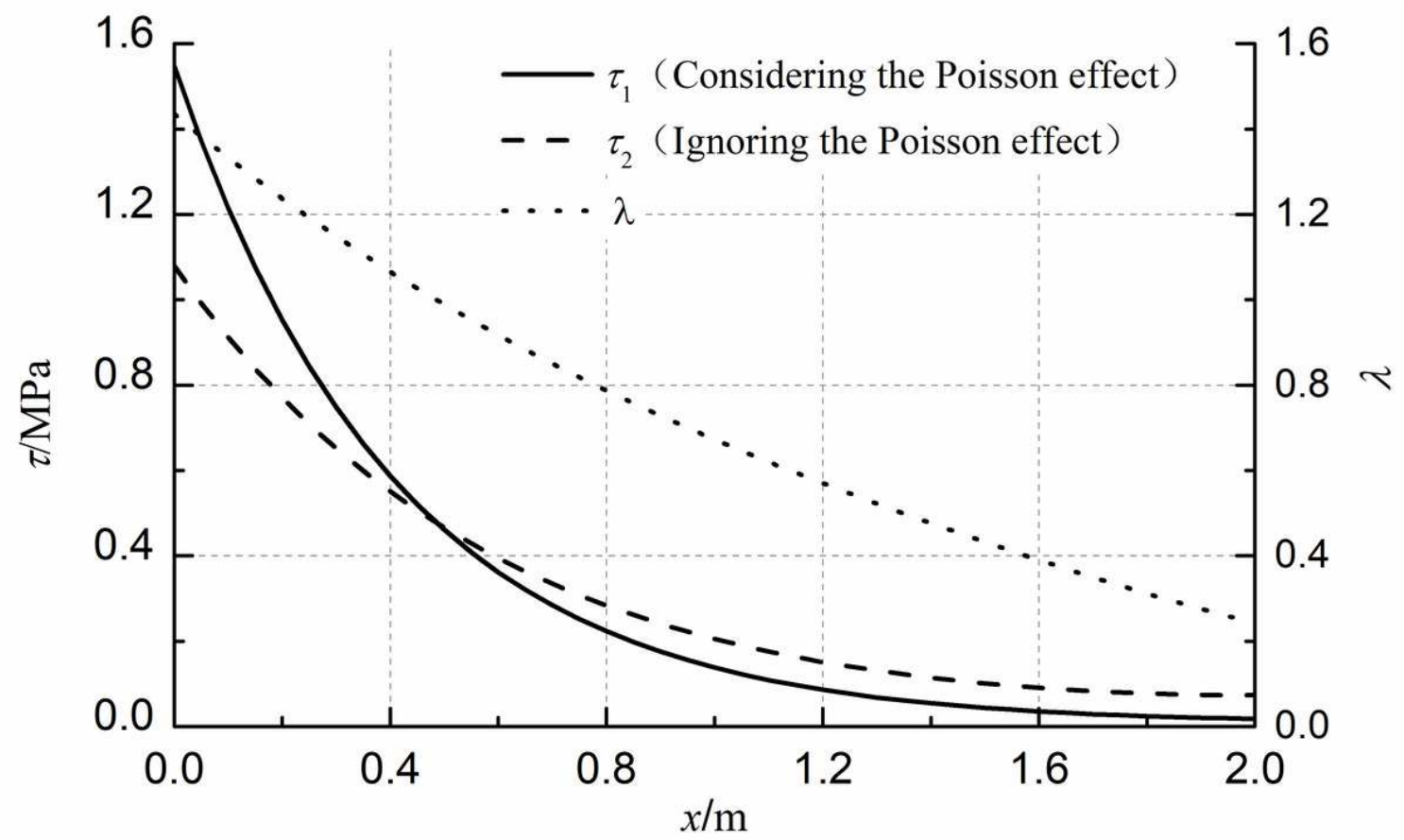

Figure 3

Distribution of shear stress and influence coefficient of Poisson effect.

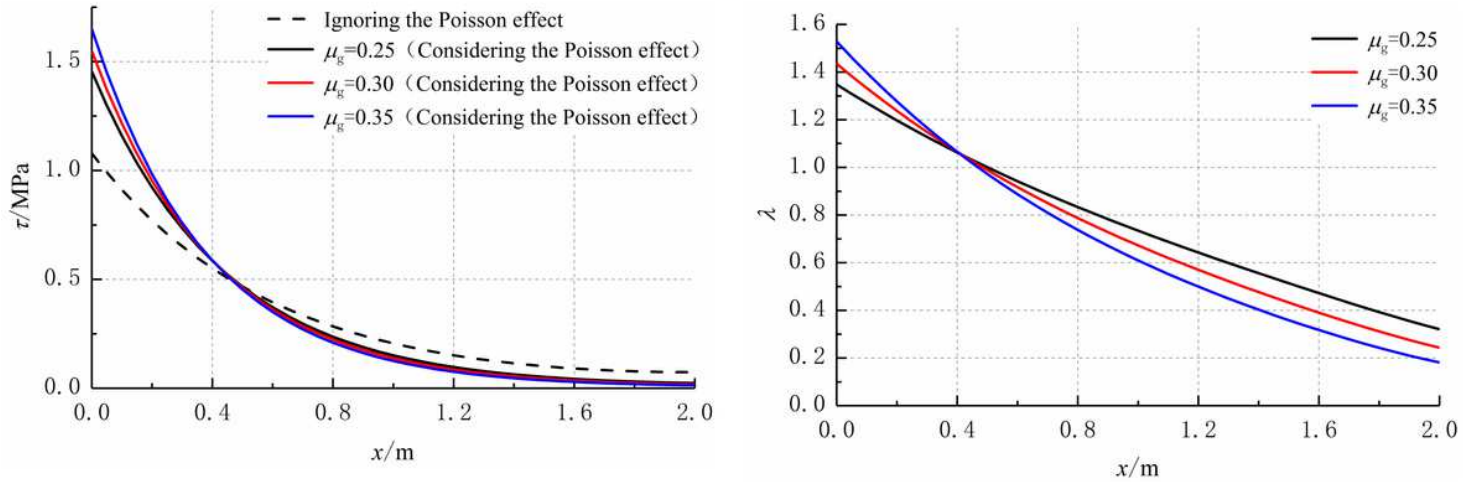

Figure 4

Influence of Poisson's ratio of grout: (a) Distribution of shear stress; (b) Distribution of influence coefficient of Poisson effect.

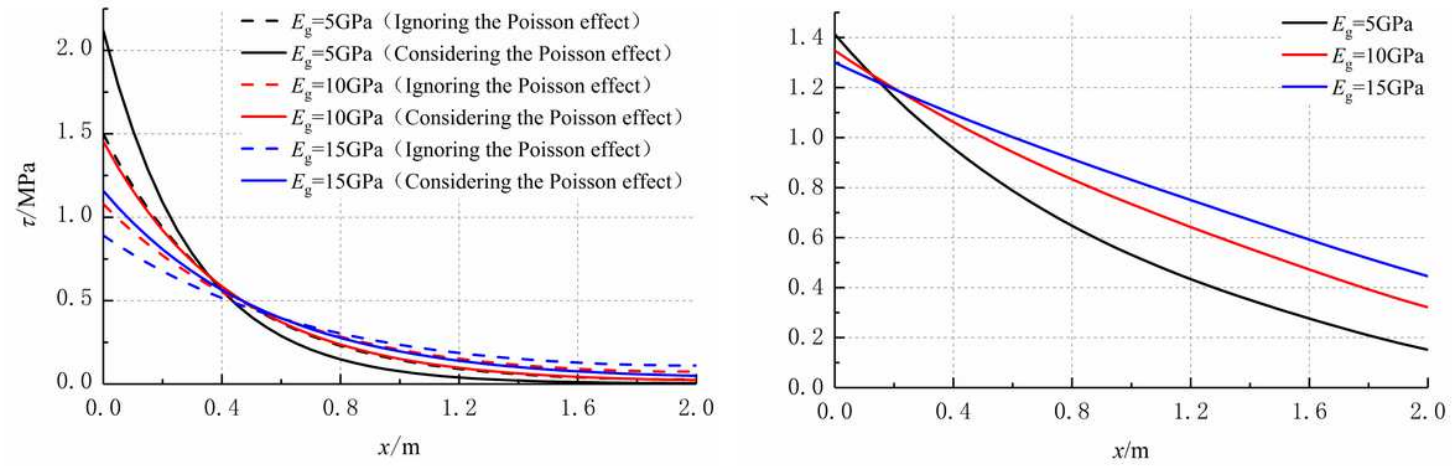

Figure 5

Influence of elastic modulus of grout: (a) Distribution of shear stress; (b) Distribution of influence coefficient of Poisson effect.

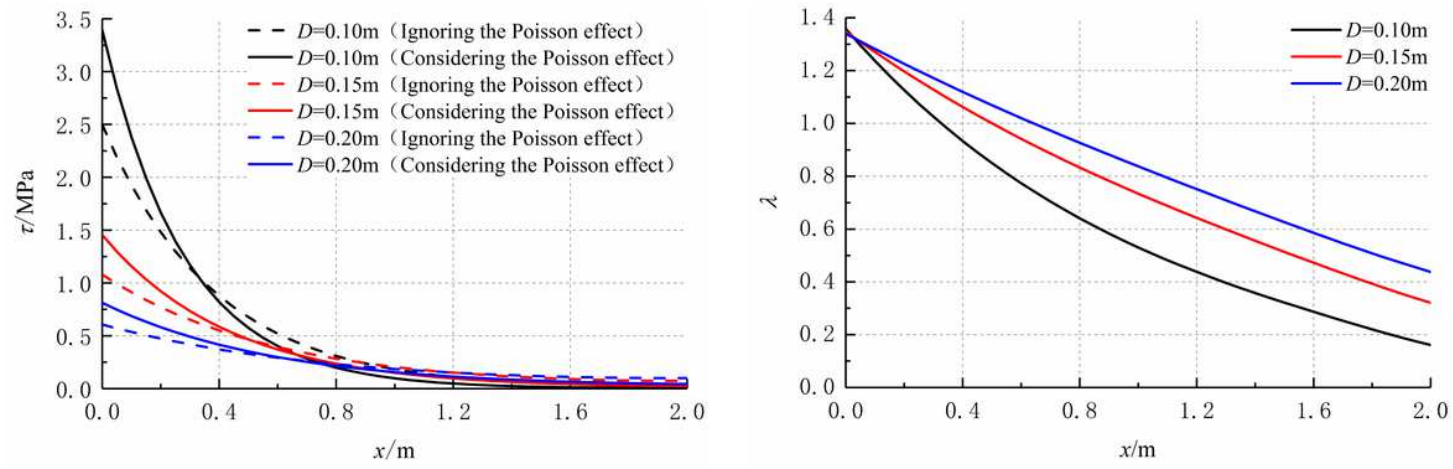

Figure 6

Influence of grout diameter: (a) Distribution of shear stress; (b) Distribution of influence coefficient of Poisson effect.

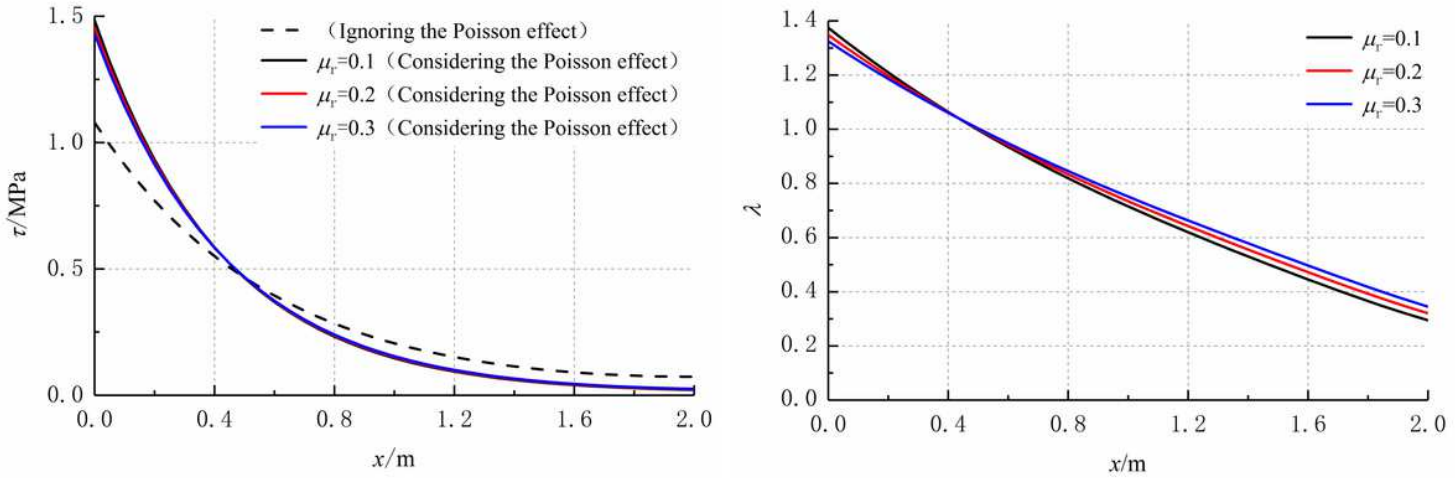

Figure 7

Influence of Poisson's ratio of rock: (a) Distribution of shear stress; (b) Distribution of influence coefficient of Poisson effect.

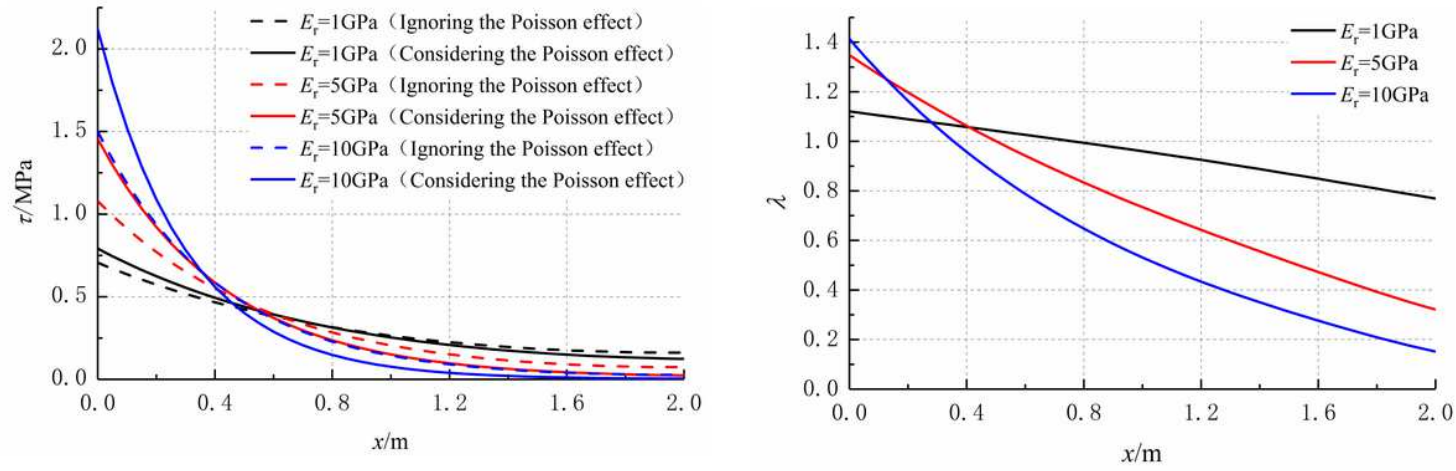

Figure 8

Influence of elastic modulus of rock: (a) Distribution of shear stress; (b) Distribution of influence coefficient of Poisson effect.

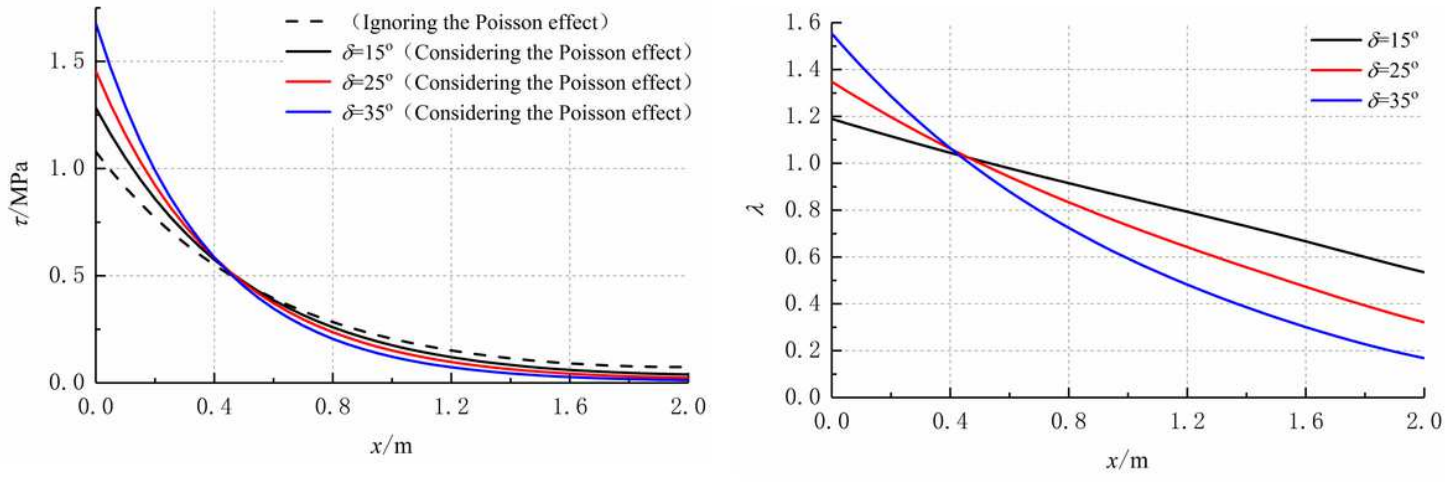

Figure 9

Influence of interface friction angle: (a) Distribution of shear stress; (b) Distribution of influence coefficient of Poisson effect.